ACS APPLIED MATERIALS & INTERFACES

Research Article

www.acsami.org

Synthesis of FeS and FeSe Nanoparticles from a Single Source Precursor: A Study of Their Photocatalytic Activity, Peroxidase-Like Behavior, and Electrochemical Sensing of H_2O_2

Amit Kumar Dutta,[†] Swarup Kumar Maji,[†] Divesh N. Srivastava,[‡] Anup Mondal,[†] Papu Biswas,*[,†] Parimal Paul,*[,‡] and Bibhutosh Adhikary*[,†]

[†]Department of Chemistry, Bengal Engineering and Science University, Shibpur, Howrah 711 103, West Bengal, India

[‡]Department of Analytical Science, Central Salt & Marine Chemicals Research Institute, Gijubhai, Badheka Marg, Bhavnagar 364002, Gujarat, India

Supporting Information

ABSTRACT: Nanocrystalline FeS and FeSe compounds were prepared by solvothermal decomposition of a precursor complex $[Fe_3(\mu_3\text{-}O)(\mu_2\text{-}O_2CCH_2Cl)_6(H_2O)_3]NO_3{\cdot}H_2O$ in the presence of thiourea and sodium selenite, respectively. The as-obtained products were characterized by X-ray diffraction analysis (XRD), field emission scanning electron microscopy (FESEM), transmission electron microscopy (TEM), and UV−vis spectroscopic techniques. Structural analyses revealed that the FeS and FeSe nanoparticles (NPs) are composed of needle-like and spherical particles, respectively. The FeS and FeSe NPs showed photocatalytic activity for the decomposition of rose bengal (RB) and methylene blue (MB) dyes under white light illumination. They also showed good catalytic activity toward oxidation of 3,3′,5,5′-tetramethylbenzidine (TMB) in the presence of H_2O_2 and followed Michaelis−Menten kinetics. In addition, both FeS and FeSe NPs exhibited electrocatalytic activity toward reduction of hydrogen peroxide, which on immobilization on glassy carbon (GC) electrodes perform as amperometric sensors for detection of H_2O_2. At pH 7.0, the FeS/GC showed a linear range for detection of H_2O_2 from 5 to 140 μM, while for FeSe/GC the range was 5 to 100 μM.

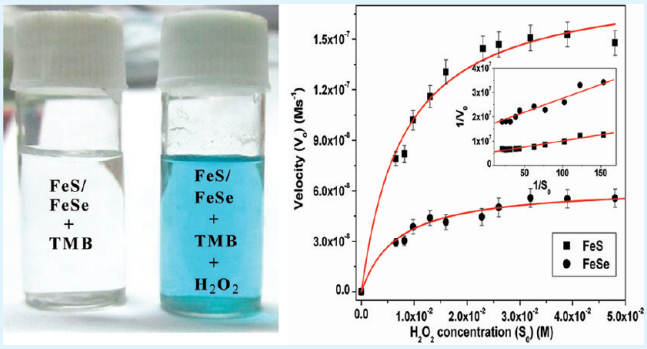

KEYWORDS: *FeS nanoparticles, FeSe nanoparticles, photocatalysis, peroxidase mimic, amperomatric biosensor*

INTRODUCTION

Over the past decades, a large number of reports have focused on the synthesis of nanoscaled inorganic materials because of their fascinating chemical and physical properties and for their application potential in devices.[1−3] Among these materials, transition metal chalcogenides represent an important family of compounds that have proved to be useful as thermoelectrics,[4] magnetic semiconductors,[5] superconductors,[6] sensors,[7] and photovoltaics.[8−10] Iron chalcogenides are of particular interest because of their interesting magnetic, semiconducting, and structural properties.[11−13] Consequently, they have been targeted for potential use in biomedical applications, including protein immobilization and separation,[14] magnetic targeting and drug delivery,[15−17] cancer hyperthermia,[18] magnetic resonance imaging (MRI),[19−21] etc. Although many reports have been published on the synthesis of FeS by various methods, in contrast, there are very few reports on the synthesis of FeSe.[22−24] Most of the methods for the synthesis of FeSe involve the use of complex apparatus, expensive chemicals, and exotic conditions. A simple, cost-effective method for the synthesis of FeSe is therefore much desired.

Decomposition of organic pollutants using nanomaterials in the presence of sun light is a topic of contemporary interest. Semiconducting nanomaterials are particularly important for this purpose because they require mild reaction condition and use at low concentrations. TiO_2 is a well-known catalyst for photodegradation of toxic organic compounds,[25−27] albeit it is catalytically active only under UV irradiation (λ < 387 nm) because of its wide band gap energy ($E_g \approx 3.2$ eV).[28] Of late, a few nontitania-based chalcogenides, such as Bi_2S_3,[29] Sb_2S_3,[30] ZnS,[31] $Co_{0.85}Se$,[32] etc., have been found to exhibit visible-light-driven catalytic activity. Obviously, there remains great demand for exploration of inexpensive materials that might be used for photodegradation of organic dyes in sun light, especially for effluents of textile wastewater. Another interesting aspect that has drawn interest of chemists is possible applications of nanoparticles (NPs) in biotechnology as biomimics of metalloenzymes. To this end, a few research groups have

Received: October 24, 2011
Accepted: March 26, 2012
Published: March 26, 2012

recently explored the peroxidase-like behavior and biosensing activity toward H_2O_2 by Fe_3O_4,[33,34] FeS,[35] CuO[36] nanomaterials, etc.

The present study is concerned with the efficient synthesis of FeS and FeSe NPs having needle-like and spherical shapes, respectively, from a trinuclear oxo-bridged iron(III) precursor complex $[Fe_3(\mu_3\text{-}O)(\mu_2\text{-}O_2CCH_2Cl)_6(H_2O)_3]NO_3{\cdot}H_2O$. We demonstrate here that both FeS and FeSe NPs exhibit efficient photocatalytic property toward degradation of rose bengal (RB) and methylene blue (MB) dyes under white light illumination. We also show for the first time the peroxidase-like activity of FeSe NPs through the oxidation of peroxidase substrate 3,3′,5,5′-tetramethylbenzidine (TMB) in the presence of H_2O_2, and a comparative study has been made with that of FeS NPs. Furthermore, when both FeS and FeSe NPs are immobilized onto the surface of glassy carbon electrodes, they demonstrate amperometric sensing of hydrogen peroxide, which again has been observed for the first time for FeSe NPs.

EXPERIMENTAL SECTION

Chemicals and Materials. All chemicals were of reagent grade and used without further purification. $Fe(NO_3)_3{\cdot}9H_2O$, chloroacetic acid, NaOH, thiourea, sodium selenite (Na_2SeO_3), anhydrous sodium acetate, and acetic acid were purchased from Spectrochem Pvt. Ltd. (India). Polyvinylpyrrolidone (PVP), hydrogen peroxide (30%), dimethyl sulfoxide (DMSO), 3,3′,5,5′-tetramethyibenzidine (TMB), rose bengal (RB), methylene blue (MB), and tungsten oxide (WO_3) were purchased from Sigma-Aldrich. Nanosized titanium dioxide (TiO_2) (Degussa-P25) was purchased from Degussa Company. Solvents were used as received.

Synthesis of the Precursor Complex $[Fe_3(\mu_3\text{-}O)(\mu_2\text{-}O_2CCH_2Cl)_6(H_2O)_3]NO_3{\cdot}H_2O$. A solution of sodium chloroacetate ($ClCH_2COOH$ (4.7 g, 50 mmol) and NaOH (2 g, 50 mmol)) in 70 mL of water was slowly added with stirring to an aqueous solution (10 mL) of $Fe(NO_3)_3{\cdot}9H_2O$ (10 g, 25 mmol). The resulting deep red solution was filtered after 3 h, and the filtrate was kept at room temperature for 2 weeks. The red crystals that deposited were filtered and washed with cold methanol and dried in air; yield 3.0 g (41%). Anal. Calcd for $C_{12}H_{20}Cl_6Fe_3NO_{20}$: C, 16.38; H, 2.27; N,1.59. Found: C, 16.45; H, 2.36; N, 1.52. IR data (KBr pellet, cm^{-1}): 3570 (m), 3280 (w, br), 1619 (s), 1430 (s), 1382(s), 1262 (m), 802 (m), 682(m), 568(s). UV−vis [in MeCN, λ_{max}, nm (ε/M^{-1} cm^{-1})] 300 (8680).

Syntheses of FeS NPs and FeSe NPs. The syntheses of FeS and FeSe NPs were carried under oxygen-free nitrogen atmosphere using the standard Schlenk technique. Water used for preparation was freed from dissolved oxygen by boiling followed by cooling under a stream of nitrogen.

Trinuclear iron(III) precursor complex $[Fe_3(\mu_3\text{-}O)(\mu_2\text{-}O_2CCH_2Cl)_6(H_2O)_3]NO_3{\cdot}H_2O$ (430 mg; 0.5 mmol) was dissolved in 30 mL of water. To this solution, 10 mL of aqueous solution containing 114 mg (1.5 mmol) of thiourea and 800 mg of PVP was added with stirring. The clear solution was then transferred into a 50 mL Teflon-lined stainless steel autoclave and kept at 150 °C in an electrical oven for 12 h. The resulting black powder of FeS was collected by centrifugation, washed several times with methanol, and finally dried in air.

To synthesize FeSe NPs, the precursor complex (430 mg, 0.5 mmol) was dissolved in 20 mL of water; then, Na_2SeO_3 (258 mg, 1.5 mmol) and PVP (800 mg) in 10 mL of distilled water were added under constant stirring. The mixture was then transferred to a stainless Teflon-lined 50 mL capacity autoclave and heated at 150 °C for 12 h. After cooling to room temperature, the black products were collected by centrifugation followed by washing several times with methanol and finally dried in air.

Fabrication of FeS and FeSe Modified Glassy Carbon Electrode. A glassy carbon (GC) electrode (3 mm diameter) was cleaned successively with 1.0, 0.3, and 0.05 μm alumina slurry (CH Instrument) followed by rinsing thoroughly with doubly distilled water and then dried at room temperature. Ten milligrams of FeS and FeSe NPs was dispersed separately in 10 mL of distilled water and then ultrasonicated for 1 h. Ten microliters of colloidal suspension was dropped on the GCE surface and dried at room temperature for overnight. Afterward, 5 μL of 1% glutaraldehyde was slowly coated onto the FeS and FeSe modified GCE surface and allowed to dry in the same condition for 1 h.

Characterization. Powder X-ray diffraction analysis (XRD) patterns were obtained on a Philips PW 1140 parallel beam X-ray diffractrometer with Bragg-Bretano focusing geometry and monochromatic Cu Kα radiation (λ = 1.540598 Å). The surface morphologies were studied using a Gemini Zeiss Supra 35VP field emission scanning electron microscope (FESEM) and JEOL JEM-2100 transmission electron microscope (TEM). N_2-sorption isotherms were obtained using a Quantachrome Instruments analyzer at 77 K. Absorption spectra and photocatalytic studies were carried out on a JASCO V-530 UV−vis spectrophotometer. Peroxidase-like activities of FeS and FeSe NPs were studied spectrophotometrically using an Agilent-8453 diode-array spectrophotometer. Electrocatalytic activities and amperometric measurements were carried out on a CHI620D electrochemical analyzer using three electrode systems.

Photocatalytic Activity Measurements. The prepared FeS and FeSe NPs were tested as a photocatalyst by the degradation of RB and MB dyes. The experiments were carried out in a round-bottom flask kept in a thermostatted bath at 22 °C, and the light source used in the measurements was an incandescent tungsten halogen lamp (200W) (emission spectrum of the incandescent tungsten halogen light is shown in Figure S1, Supporting Information), placed vertically on the reaction vessel at a distance of ∼10 cm. The catalytic experiments were separately carried out with 40 mL of aqueous solution of RB (6.6×10^{-5} M) or MB (6×10^{-6} M) using 20 mg of the catalyst (FeS and FeSe NPs). To obtain the adsorption−desorption equilibrium states in RB/MB, the suspensions were magnetically stirred in the dark for 30 min prior to light irradiation. During irradiation, 3 mL of aliquot was withdrawn at specific time intervals and centrifuged. The clear solutions of the dyes were measured on a UV−vis spectrophotometer in the range of 400−600 nm for RB and 550−750 nm for MB, respectively. Commercial photocatalysts TiO_2 and WO_3 were also used as the reference to compare the photocatalytic activity under the same experimental conditions.

Peroxidase-Like Activity Measurements. To investigate the peroxidase-like activity of FeS and FeSe NPs, the catalytic oxidation of the peroxidase substrate TMB in acetate buffer solution was carried out in the presence of H_2O_2. To examine the capability of FeS or FeSe as catalyst for the oxidation of TMB, a 3.0 mL solution of sodium acetate (0.1 M and pH 4.0) containing 2.4 μL of 0.125 M TMB (dissolved in DMSO) was successively treated with (i) 20 μg of FeS or FeSe, (ii) 4 μL of 30% H_2O_2, and (iii) 4 μL of 30% H_2O_2 with 20 μg FeS or FeSe. All the reactions were monitored spectrophotometrically in time-scan mode at 653 nm. The kinetic analyses of FeS and FeSe NPs with TMB as substrate were performed using 20 μg of FeS or FeSe with fixed concentration of H_2O_2 (13 mM) and varying concentrations of TMB (0, 10.4, 14.5, 20, 40, 60, 80, and 120 μM). Similarly, the kinetic analyses with H_2O_2 as the substrate were performed using 20 μg of FeS or FeSe with fixed concentration of TMB (100 μM) and varying concentration of H_2O_2 (0, 6.5, 8.2, 9.8, 13, 16, 23, 26, 32, 39, 48 mM). Apparent kinetic parameters were calculated on the basis of the Michaelis−Menten equation

$$V_0 = \frac{V_{max}[S]}{K_m^{app} + [S]} \quad (1)$$

V_0 is the initial catalytic rate, V_{max} is the maximum rate conversion, which is attained when the catalytic sites on the enzyme are saturated with substrate, $[S]$ is the substrate concentration, and K_m^{app} is the apparent Michaelis−Menten constant.

Electrochemical H_2O_2 Measurements. Electrochemical experiments were carried out under nitrogen atmosphere by cyclic voltammetric technique in a cell containing 20.0 mL of 0.1 M phosphate buffer solution (PBS) with FeS or FeSe modified glassy

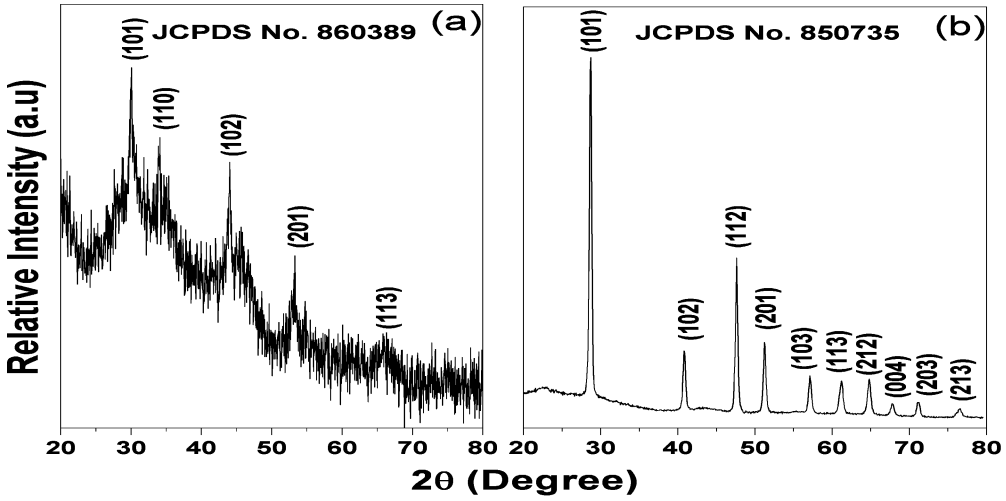

Figure 1. XRD patterns of (a) FeS and (b) FeSe NPs.

carbon electrode (FeS/GC or FeSe/GC) as working electrode, platinum wire counter electrode, and an Ag/AgCl reference electrode at room temperature at a scan rate of 0.1 V s^{-1}. Phosphate buffer solutions (0.1 M) of pH ranging from 2 to 10 were prepared by mixing stock standard solutions of Na_2HPO_4, and the pH was adjusted with H_3PO_4 or NaOH. In this experiment, the current−potential data was recorded after successive addition of H_2O_2 into the buffer solution at optimum conditions (pH and temperature). The sensor response was measured as increasing reduction peak current.

For amperometric detection, all measurements were performed by applying an appropriate potential, −0.4 V on FeS/GC and −0.5 V on FeSe/GC (vs Ag/AgCl). The current responses due to the addition of H_2O_2 in the stirred PBS were recorded. The Michaelis−Menten constant, K_m^{app} and the maximum current (I_{max}) of FeS/GC and FeSe/GC electrodes can be determined from the Michaelis−Menten equation,

$$I = \frac{I_{max}[S]}{K_m^{app} + [S]} \quad (2)$$

where I is the steady-state current, I_{max} is the maximum current measured under conditions of enzyme saturation, $[S]$ is the concentration of substrate, and K_m^{app} is the apparent Michaelis−Menten constant. Rearrangement of the Michaelis−Menten equation yields the electrochemical version of the Lineweaver−Burk equation,[37] which also enables the analysis of the enzyme kinetics.

$$\frac{1}{I} = \frac{1}{I_{max}} + \frac{K_m^{app}}{I_{max} \times [S]} \quad (3)$$

RESULTS AND DISCUSSION

Preparation of the FeS and FeSe NPs. The reaction between the aqueous solution of precursor complex and thiourea or sodium selenite (Na_2SeO_3) in 1:3 molar ratio at 150 °C under pressure for 12 h leads to the formation of FeS or FeSe as black powder. Apparently, the reduction of iron(III) to iron(II) and concomitant formation of FeS or FeSe take place via multiple reaction steps. In the absence of detailed product analysis, no attempt has been made to speculate on the reaction mechanisms involved.

A number of methods have been reported in the literature for the preparation of FeS and FeSe nanoparticles. We have been on the lookout of a precursor complex that can be used for the synthesis of Fe_2O_3, Fe_3O_4, FeS, FeSe, and FeTe NPs in different morphologies. For this purpose, we find that the trinuclear oxo-bridged $[Fe_3(\mu_3\text{-}O)(\mu_2\text{-}O_2CCH_2Cl)_6(H_2O)_3]^+$ core serves as an excellent precursor for the synthesis of iron chalcogenides.

The concentrations of iron and sulfide/selenide ions have to be controlled very carefully during the deposition of nanoparticles. This can be easily achieved using a complex with high stability and a moderately stable sulfur/selenium source. Here, a water-soluble trinuclear oxo-bridged $[Fe_3(\mu_3\text{-}O)(\mu_2\text{-}O_2CCH_2Cl)_6(H_2O)_3]^+$ core has been employed as a precursor complex, thiourea and sodium selenite as sulfur and selenium source, respectively. In the reaction system, water-soluble trinuclear iron core facilitated the slow release of iron ion and thus controlled its concentration. In this context, it can be mentioned that, according to Qu et al.,[38] the metal salts with an anion of a weak acid are all presumably excellent precursor for metal ion sources. The existence of any anion of a strong acid often made it difficult to form metal chalcogenides, so our water-soluble iron core with chloroacetate anion, as a substitute of common iron salts, is a better precursor in many ways. Another important advantage of this precursor complex is the pH of its aqueous solution that lies in between 2.5 and 3.0, which is also suitable[39] for the deposition of iron chalcogenides.

Structural Characterization. The crystallinity and purity of FeS and FeSe NPs were examined by the X-ray diffraction (XRD) technique. As shown in Figure 1, the diffraction patterns of both the powder materials can be indexed into pure FeS and FeSe phase crystallizing in the *P*4/*nmm* space group. The observed peaks are in good agreement with those reported for pure tetragonal phase of FeS (JCPDS card no. 860389) and FeSe (JCPDS card no. 850735).

The surface morphologies of the as-synthesized FeS and FeSe NPs were investigated by field emission scanning electron microscopy (FESEM). Figure 2 presents the corresponding FESEM images of the products in which FeS exhibits needle-like morphology having length of 50−200 nm and about 3−5 nm thicknesses. On the other hand, FeSe NPs displayed quasi-spherical morphology (Figure 2b) with average diameter of 6 nm.

To provide additional insight into the structure of the as-prepared nanomaterials, TEM analyses were carried out. Typical TEM image in Figure 3a illustrates that the FeS NPs are needle-like nanostructures with thickness of approximately 3−5 nm and edge lengths ranging from 50 to 200 nm. On the other hand, FeSe NPs are spherical in shape with average

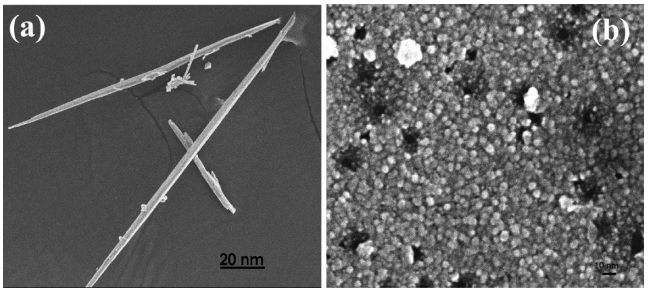

Figure 2. FESEM images of as-prepared (a) FeS and (b) FeSe NPs.

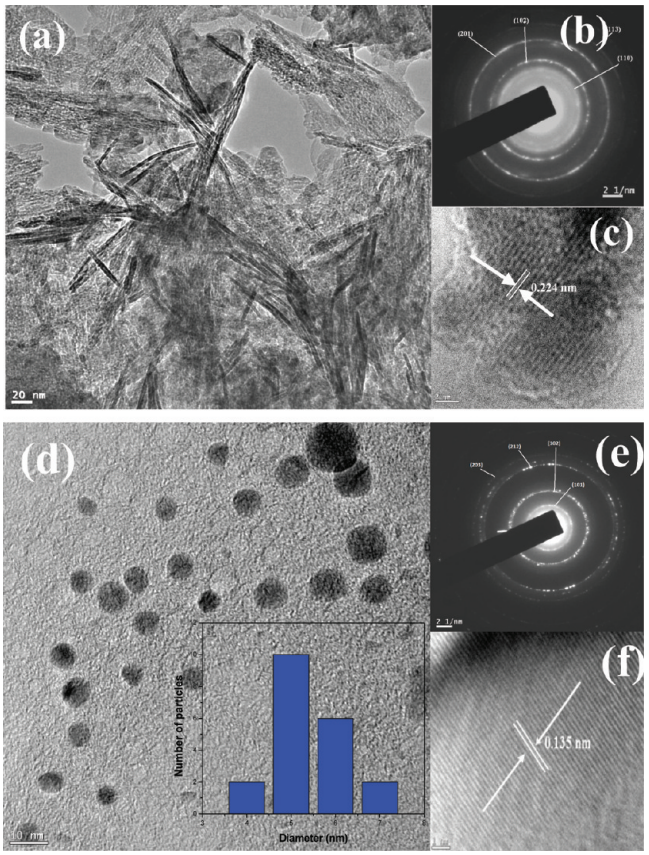

Figure 3. (a) TEM image, (b) SAED pattern, and (c) HRTEM image of FeS NPs. (d) TEM image (inset: particle size distribution), (e) SAED pattern, and (f) HRTEM image of FeSe NP.

diameter of about 6 nm (Figure 3d); albeit, the particles have a broader size distribution ranging from 4 to 10 nm (Figure 3d inset). Selected area electron diffraction (SEAD) patterns of FeS and FeSe NPs (Figure 3b,e) exhibit concentric rings that can be indexed to (110), (102), (201), and (113) diffraction planes for primitive tetragonal FeS and (101), (102), (212), and (203) diffraction planes for primitive tetragonal FeSe, respectively. These findings are consistent with the observations made from the XRD patterns. From the HRTEM images of FeS and FeSe NPs (Figure 3c,f), it is obvious that the surface in an individual FeS and FeSe NP is single crystalline with a lattice fringe spacing of 0.224 and 0.135 nm corresponding to the (102) and (112) planes, respectively.

It should be noted that there are several forms of iron sulfides other than FeS, namely, $Fe_{1-x}S$, Fe_7S_8, Fe_9S_{10}, Fe_3S_4, and FeS_2. Similarly, iron selenide occurs as $FeSe_2$, Fe_3Se_4, and Fe_7Se_8. The results obtained from XRD and TEM measurements clearly indicate that FeS and FeSe obtained in the present study are phase pure tetragonal nanocrystallites with two different morphologies.

Optical Properties. Optical properties of both FeS and FeSe NPs were investigated by UV–vis spectroscopic techniques and are displayed in Figure 4. From the recorded

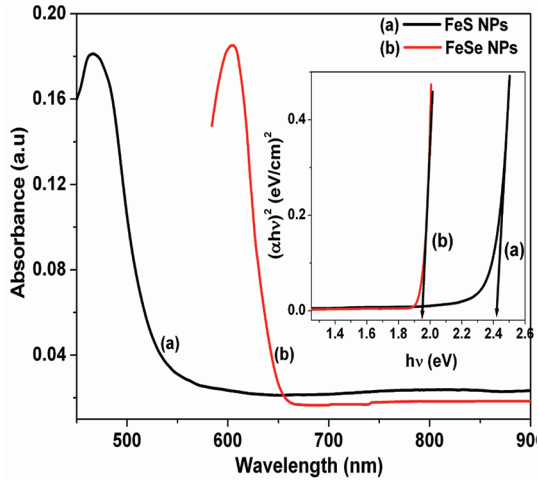

Figure 4. UV–vis spectrum of the as-synthesized FeS and FeSe NPs. Inset: corresponding Tauc plot.

optical spectra, the band gap energies (E_g) of FeS and FeSe have been estimated using the Tauc's relation[40] (Figure 4 inset), which are found to be 2.43 eV for FeS and 1.95 eV for FeSe. The large blue shifts observed for the optical spectra of FeS and FeSe NPs from their corresponding bulk materials (from 0.9 to 2.43 eV for FeS and 1.2 to 1.95 eV for FeSe)[39b,41] are probably due to the well-known quantum confinement effect.[42] Since the band gap energies of FeS and FeSe NPs fall in the solar spectrum range,[30,43] they can be easily activated by visible light for photocatalytic reactions.

N_2-Sorption Studies. Brunauer–Emmett–Teller (BET) measurements were carried out to know the porous nature and specific surface area of FeS or FeSe NPs. Typical nitrogen adsorption–desorption isotherms at 77 K and the corresponding pore size distributions are presented in Figure 5. All the isotherms are identified as type IV isotherm, with a H_2-type

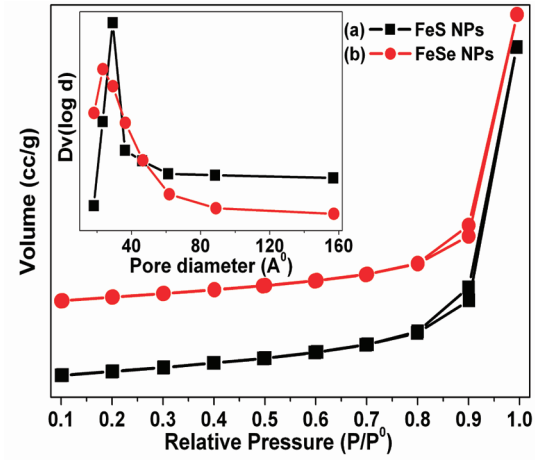

Figure 5. BET isotherms and in inset corresponding pore size distribution curves of FeS and FeSe NPs.

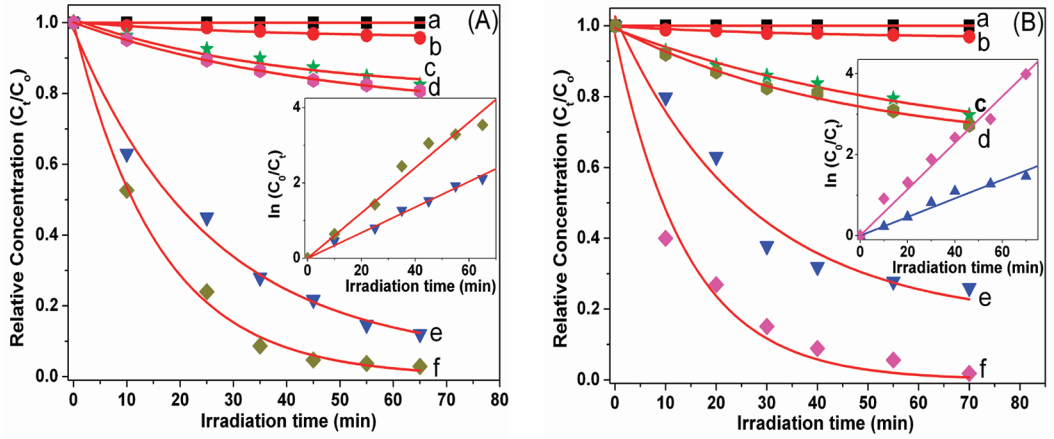

Figure 6. Photocatalytic degradation following pseudofirst order kinetics of (A) rose bengal and (B) methylene blue under different conditions: (a) without catalyst in dark, (b) without catalyst in light, (c) commercial TiO_2 in light, (d) commercial WO_3 in light, (e) FeSe NPs in light, (f) FeS NPs in light. Inset: corresponding kinetic plots.

hysteresis, confirming the mesoporous structures. The porosity of these NPs was determined from pore-size distribution curves (Figure 5 inset) and shows the sharp distribution in the mesoporous region. The average pore diameter according to the Bopp–Jancso–Heinzinger (BJH) method of both the samples were found to be 29 nm (for FeS NPs) and 23 nm (for FeSe NPs), and specific surface areas of FeS and FeSe NPs are 25.5 and 20.2 $m^2\ g^{-1}$, respectively.

Photocatalytic Activity. The photocatalytic activity was studied by monitoring the absorption intensity of RB and MB, which decreases rapidly with the irradiation time (Figure S2, Supporting Information). The time dependent relative concentration changes of the dyes with the catalysts FeS, FeSe, TiO_2, and WO_3 and in absence of catalysts are compared in Figure 6A(for RB),B(for MB). The decomposition processes have been modeled as a pseudofirst order reaction with the kinetics expressed by the equation $\ln(C_0/C_t) = kt$, where C_0 represents the initial concentration, C_t denotes the concentration at a given reaction time "t", and k is the reaction rate constant. From the linear extrapolations (Figure 6 insets), the reaction rate constants have been obtained and are given in Table 1. From the rate constant values, it can be seen that degradation of both the dyes occurs faster with FeS than FeSe NPs. The enhanced catalytic activity of FeS NPs can be correlated with the higher specific surface area. A larger specific surface area allows more dye molecules to be adsorbed onto the surface of the photocatalyst, thereby enhancing the rate of degradation. The results of the BET analyses revealed that the surface area of FeS NPs is larger than that of FeSe NPs, which is well matched with the result of photocatalytic decomposition of RB and MB. It is worthy to note that the catalytic activities of both iron-based nanoparticles are significantly better than that of commercial TiO_2 and WO_3.

Table 1. Comparison of the Rate Constants of FeS, FeSe, TiO_2, and WO_3

photocatalyst	rate constant (RB) (min^{-1})	rate constant (MB) (min^{-1})
FeS	6.02×10^{-2}	5.73×10^{-2}
FeSe	3.39×10^{-2}	2.32×10^{-2}
TiO_2	3.18×10^{-3}	4.35×10^{-3}
WO_3	3.29×10^{-3}	4.43×10^{-3}

In addition, the stability of FeS and FeSe NPs were also examined by pursuing the RB degradation process with the same FeS and FeSe samples for five successive reactions. Slight decreases in the catalytic activity (97% to 92% for FeS and 88% to 82% for FeSe) (Figure S3, Supporting Information) were observed for both the materials after these successful reuses. Therefore, it is also established that our prepared FeS and FeSe NPs are stable enough for degradation reactions at normal conditions.

Steady-State Kinetic Analysis of Peroxidate Substrate Oxidation. Peroxidase-like behaviors of the synthesized NPs were investigated spectrophotometrically at room temperature using TMB as the peroxidase substrate. Upon addition of FeS or FeSe NPs to H_2O_2 and TMB, a blue color change occurs, indicating peroxidase-like catalytic reaction. Similar to the enzymatic peroxidase activity observed for the enzyme HRP,[33a] this color reaction was quenched by adding H_2SO_4 (Figure 7a inset). The reaction was monitored by following the increase of absorbance at 653 nm with time (Figure 7a), which originated from the oxidation product of TMB. Figure 7b presents the time course curves of the different reaction systems catalyzed by FeS and FeSe NPs within 130 s. The observed reaction rates indicate better catalytic activity of FeS compared to that of FeSe NPs.

The kinetic parameters for the reaction were evaluated by the initial rate method. The absorbance data were converted to corresponding concentration term using the value ε = 39000 $M^{-1}cm^{-1}$ (at 653 nm) for the oxidized product of TMB.[44] Within the suitable range of TMB (Figure 8a) and H_2O_2 (Figure 8b) concentrations, typical Michaelis–Menten curves were observed for both FeS and FeSe NPs. The data were fitted to the Michaelis–Menten model to obtain the catalytic parameters given in Table 2. All these parameters were also evaluated from the Lineweaver–Burk[45] double-reciprocal plot ($1/V_0$ vs $1/S_0$), which gave analogous values (Figure 8a,b insets).

The apparent Michaelis–Menten constant (K_m^{app}, which is the affinity of the enzyme to the substrate) with TMB as the substrate for FeS is slightly lower than that of FeSe NPs and significantly lower than that of HRP.[33a] The lower K_m^{app} value for FeS suggest that it has higher affinity than that of FeSe and HRP toward TMB. On the other hand, the K_m^{app} values of FeS and FeSe NPs with H_2O_2 as substrate are 9.36 and 8.09 mM,

dx.doi.org/10.1021/am300408r | ACS Appl. Mater. Interfaces 2012, 4, 1919–1927

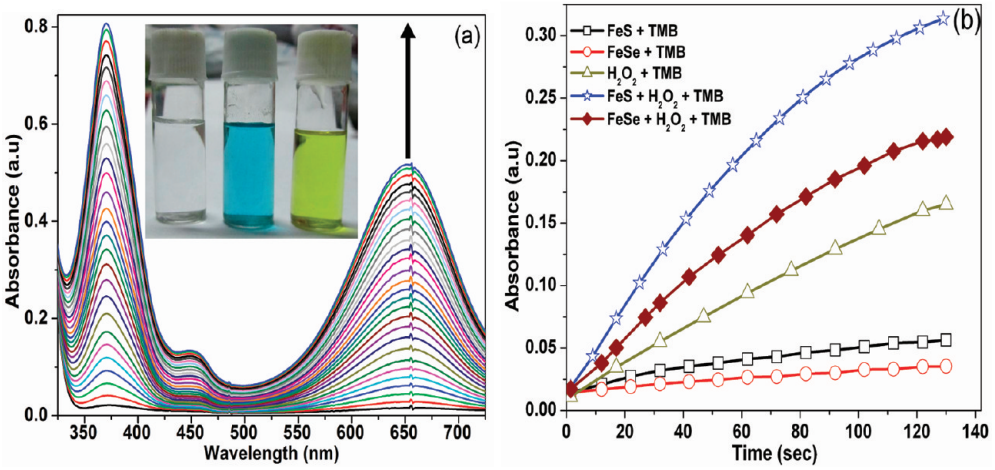

Figure 7. (a) Time dependent UV–vis spectral changes of TMB-H_2O_2 system catalyzed by FeS or FeSe NPs. Inset: Typical photography of TMB reaction system (from left to right: with only catalyst nanoparticles (colorless), with H_2O_2 after catalytic reaction by nanoparticles (blue color), the same reaction system after adding H_2SO_4 to quench this catalytic reaction (yellow color)). (b) UV–vis absorption-time course curve of TMB using FeS or FeSe NPs under different conditions.

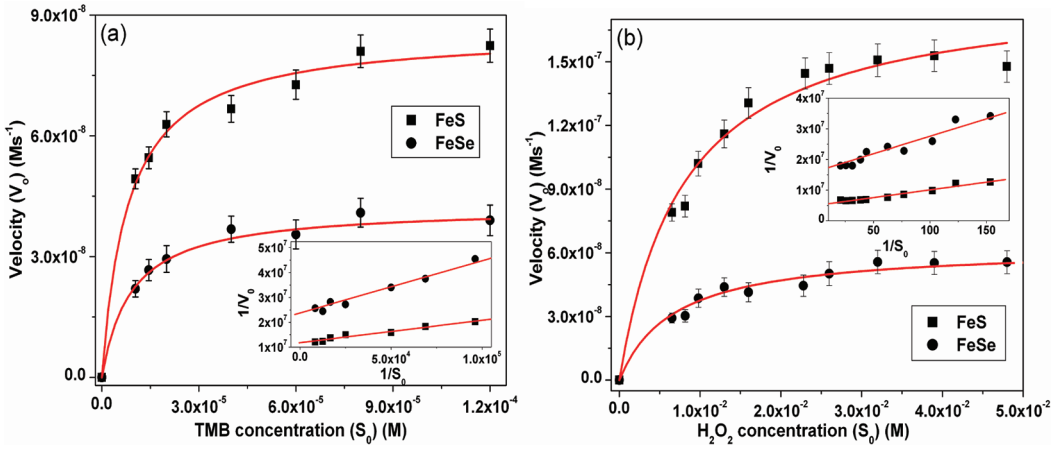

Figure 8. Steady-state kinetic analyses using the Michaelis–Menten model and Lineweaver–Burk model (insets) for (■) FeS (●)FeSe nanoparticles by (a) varying the concentration of TMB with fixed amount of H_2O_2 and (b) varying the concentration of H_2O_2 with fixed amount of TMB.

Table 2. Kinetic Parameters for the Peroxidase-Like Activity of FeS, FeSe NPs, and HRP

	substrate	K_m^{app}(mM)	V_{max} (Ms^{-1})
FeS	TMB	0.0082	8.7×10^{-8}
	H_2O_2	9.36	1.92×10^{-7}
FeSe	TMB	0.0089	4.22×10^{-8}
	H_2O_2	8.09	6.51×10^{-8}
HRP[33a]	TMB	0.434	10.0×10^{-8}
	H_2O_2	3.7	8.71×10^{-8}

respectively, which are three times higher than that of HRP[33a] suggesting that a higher amount of H_2O_2 is required to achieve the maximum activity.

Electrocatalytic Activity toward Reduction of H_2O_2. In order to use FeS and FeSe NPs as electrochemical sensors for H_2O_2, the nanoparticles have been immobilized on glassy carbon electrode surface. Over the pH range of 2.0 to 10.0 and temperature range of 20 to 80 °C, maximum electrocatalytic decomposition of H_2O_2 occurs at pH 7.0 and at 40 °C for both FeS/GC and FeSe/GC. Figure 9a,b shows the cyclic voltammograms of FeS/GC and FeSe/GC electrodes in 0.1 M, pH 7.0 PBS with different amounts of H_2O_2. In absence of H_2O_2, both FeS/GC and FeSe/GC show one reduction peaks located at around −0.4 and −0.5 V, respectively. Upon addition of H_2O_2, the reduction peak current increases dramatically, indicating obvious electrocatalytic behavior of both nanomaterials toward reduction of H_2O_2.

Amperometric Response to Hydrogen Peroxide. To demonstrate the efficacy of the FeS and FeSe NPs as biosensors, hydrogen peroxide is used as a control system to perform amperometric experiments via a three-electrode setup in 20 mL of PBS. The biosensors serve as the working electrode, a platinum wire as the auxiliary electrode, and Ag/AgCl as the reference electrode. The amperometric responses of FeS/GC and FeSe/GC at a working potential of −0.4 and −0.5 V (vs Ag/AgCl) in 0.1 M PBS (pH 7.0) for each successive addition of various amounts of H_2O_2 are presented in Figure 10a,b. Upon each addition of H_2O_2, electrochemical responses were recorded while the solution was stirred constantly. As shown in Figure 10a,b, it is clear that, when an aliquot of H_2O_2 is added to the PBS (pH 7.0), reduction current of FeS/GC and FeSe/GC increase sharply to reach a steady-state value (ca. 95%) in less than 10 s.

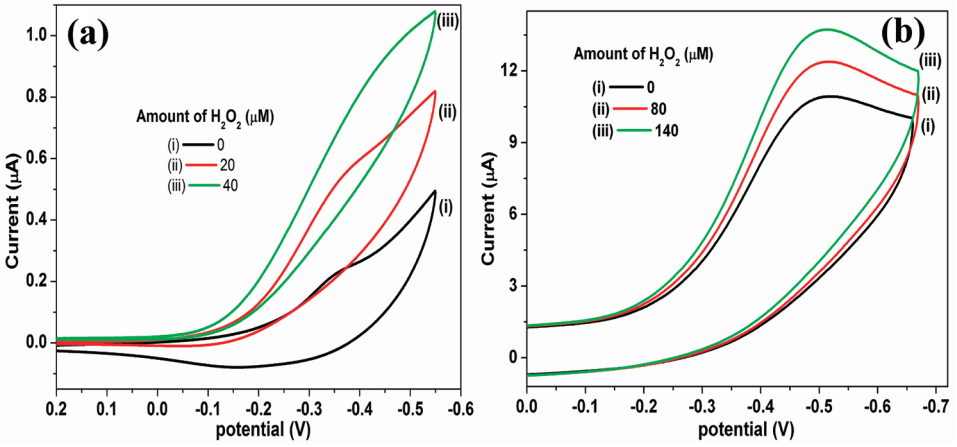

Figure 9. Cyclic voltammograms of (a) FeS and (b) FeSe modified GC electrodes in 0.1 M PBS containing various amounts of H_2O_2 at 0.1 V s^{-1} (vs Ag/AgCl).

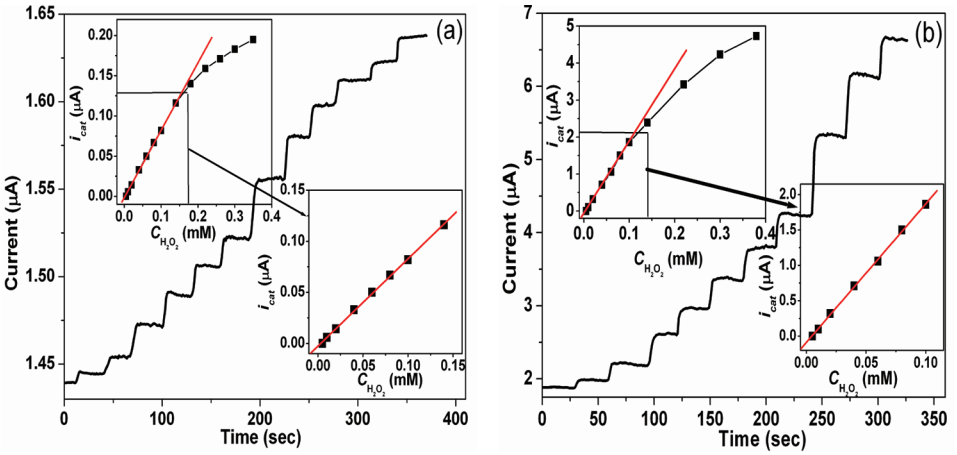

Figure 10. Amperometric responses of (a) FeS/GC and (b) FeSe/GC electrodes upon successive addition of different amounts of H_2O_2 to PBS. Insets: calibration curves of amperometric response with H_2O_2 concentration (upper left) and magnified linear regions (lower right).

From the calibration curves, (upper left insets of Figure 10a,b) between amperometric current and concentration of H_2O_2, a linear relationship for FeS/GC has been obtained in the concentration range of 5 to 140 μM (correlation coefficient of 0.9996) with sensitivity of 0.85 μA mM^{-1} (lower right inset Figure 10a), while the FeSe/GC electrode showed the linear range from 5 to 100 μM (correlation coefficient 0.998) with sensitivity of 19.57 μA mM^{-1} (lower right inset Figure 10b). The detection limits were estimated to be 4.3 and 3 μM for FeS/GC and FeSe/GC electrodes, respectively (signal-to-noise ratio 3).

As the general enzymatic reaction, the calibration curves of the FeS nanoneedles and FeSe nanospheres at H_2O_2 concentrations higher than 140 and 100 μM, respectively, show Michaelis–Menten type behavior. The apparent Michaelis–Menten constants (K_m^{app}) have been obtained from the electrochemical version of Lineweaver–Burk model, and the amperometric response parameters are compared in Table 3. The experimental results illustrate that the FeS/GC electrode showed an enhance electrochemical behavior compared to that of FeSe/GC electrode, which can be correlated with the specific surface area of the nanomaterials and matched well with results of photocatalytic decomposition of dyes.

In addition, morphological stability of FeS and FeSe NPs after the electrochemical measurements was examined by TEM analyses. As shown in Figure S4, Supporting Information, the TEM images for both the NPs seem to remain unchanged as compared to that of as-prepared nanomaterials.

Table 3. Comparison of Amperometric Response Parameters of FeS/GC and FeSe/GC

electrode	surface area (m^2g^{-1})	sensitivity (μA mM^{-1})	linear range (μM)	detection limit (μM)	K_m^{app} (mM)
FeS (needle)/GC	25.5	0.85	5–140	4.3	1.43
FeSe (sphere)/GC	20.2	19.57	5–100	3.0	2.59

CONCLUSIONS

In conclusion, nanosized FeS and FeSe materials have been successfully prepared from a trinuclear iron(III) precursor complex $[Fe_3(\mu_3\text{-}O)(\mu_2\text{-}O_2CCH_2Cl)_6(H_2O)_3]NO_3{\cdot}H_2O$ by a simple hydrothermal decomposition process. The prepared FeS and FeSe NPs act as photocatalysts for degradation of RB and MB dyes and show higher catalytic activities than that of commercial TiO_2 and WO_3. Moreover, the rate constants for degradation of the dyes in the presence of FeS NPs are higher than that of FeSe NPs. The FeSe NPs illustrate the intrinsic

dx.doi.org/10.1021/am300408r | ACS Appl. Mater. Interfaces 2012, 4, 1919–1927

peroxidase-like activity by following the Michaelis–Menten kinetics and have nearly similar affinity to peroxidase substrates TMB and H_2O_2 in comparison to that of FeS NPs. Both the FeS and FeSe NPs immobilized on glassy carbon electrode show electrocatalytic activity toward reduction of H_2O_2 and perform as good amperometric sensors for hydrogen peroxide. To the best of our knowledge, it is the first report on peroxidase like activity and amperometric sensing of H_2O_2 using FeSe NPs and can be used as enzyme-mimetic, which will facilitate the utilization in environmental chemistry, medical diagnostics, and biotechnology.

■ ASSOCIATED CONTENT

Supporting Information

Emission spectrum of incandescent tungsten halogen light (Figure S1); UV–vis spectral changes of RB and MB (Figure S2); cyclic runs in the photocatalytic degradation of RB (Figure S3); TEM images of FeS and FeSe NPs after electrochemical measurements (Figure S4). This material is available free of charge via the Internet at http://pubs.acs.org.

■ AUTHOR INFORMATION

Corresponding Author

*E-mail: bibhutoshadhikary@yahoo.in (B.A.). Tel.: +91-033-2668-4561-64 ext: 512 (B.A.). Fax: +91-033-2668-2916 (B.A.). E-mail: biswaspapu@rediffmail.com (P.B.). Tel.: +91-033-2668-4561-64 ext: 517 (P.B.). Fax: +91-033-2668-2916 (P.B.). E-mail: ppaul@csmcri.org (P.P). Tel.: +91-0278-2567760 ext: 660 (P.P.).

Notes

The authors declare no competing financial interest.

■ ACKNOWLEDGMENTS

Authors are thankful to Prof. K. Nag (IACS, Kolkata) for helpful discussion. Also we thank Prof. N. R. Bandyopadhyay (BESUS, Howrah) for providing instrumental facilities. A.K.D. and S.K.M. are indebted to UGC, India, and CSIR, India, for their SRF [11-2/2002 (SA-I)] and [08/003(0089)/2012-EMR-I], respectively. P.B. acknowledges DST for the Fast Track Project (No.SR/FT/CS-022/2009). B.A. also acknowledges CSIR (01(1912)/04/EMR-II) for financial support. The authors acknowledge the facility developed in the Department of Chemistry, BESUS through MHRD (India) and UGC-SAP (India).

■ REFERENCES

(1) Sardar, K.; Rao, C. N. R. *Adv. Mater.* **2004**, *16*, 425.
(2) Rao, C. N. R.; Deepak, F. L.; Gundiah, G.; Govindaraj, A. *Prog. Solid State Chem.* **2003**, *31*, 5.
(3) Hu, J. T.; Odom, T. W.; Lieber, C. M. *Acc. Chem. Res.* **1999**, *32*, 435.
(4) Wood, C. *Rep. Prog. Phys.* **1988**, *51* (4), 459.
(5) Dietl, T. *Semicond. Sci. Technol.* **2002**, *17* (4), 377.
(6) Niu, H. J.; Hampshire, D. P. *Phys. Rev. B* **2004**, *69* (17), 9.
(7) Schoning, M. J.; Kloock, J. P. *Electroanalysis* **2007**, *19* (19–20), 2029.
(8) Ennaoui, A.; Fiechter, S.; Pettenkofer, C.; Alonsovante, N.; Buker, K.; Bronold, M.; Hopfner, C.; Tributsch, H. *Sol. Energy Mater. Sol. Cells* **1993**, *29* (4), 289.
(9) Huynh, W. U.; Dittmer, J. J.; Alivisatos, A. P. *Science* **2002**, *295* (5564), 2425.
(10) Mitzi, D. B.; Yuan, M.; Liu, W.; Kellock, A. J.; Chey, S. J.; Deline, V.; Schrott, A. G. *Adv. Mater.* **2008**, *20* (19), 3657.
(11) Bonneau, P. R.; Jarris, R. R., Jr.; Kaner, R. B. *Nature* **1991**, *349*, 510.
(12) Ferrer, I. J.; Caballero, F.; Delas, H. C.; Sarchez, C. *Solid State Commun.* **1994**, *89*, 349.
(13) Tang, K. B.; Qian, Y. T.; Zeng, J. H.; Yang, X. G. *Adv. Mater.* **2003**, *15*, 448.
(14) (a) Perez, J. M.; Simeone, F. J.; Tsourkas, A.; Josephson, L.; Weissleder, R. *Nano Lett.* **2004**, *4*, 119. (b) Oscar, B. M.; Maria, P. M.; Pedro, T.; Jesus, R. C.; Pierre, B.; Martin, S.; Zhao, X. Q.; Sabino, V. V. *Biomaterials* **2005**, *26*, 5695.
(15) Cheng, J. J.; Teply, B. A.; Jeong, S. Y.; Yim, C. H.; Ho, D.; Sherifi, I.; Jon, S.; Farokhzad, O. C.; Khademhosseini, A. R.; Langer, S. *Pharm. Res.* **2006**, *23*, 557.
(16) Yang, Y.; Jiang, J. S.; Du, B.; Gan, Z. F.; Qian, M.; Zhang, P. *J. Mater. Sci.: Mater. Med.* **2009**, *20*, 301.
(17) Gou, M. L.; Qian, Z. Y.; Wang, H.; Tang, Y. B.; Huang, M. J.; Kan, B.; Wen, Y. J.; Dai, M.; Li, X. Y.; Gong, C. Y.; Tu, M. J. *J. Mater. Sci.: Mater. Med.* **2008**, *19*, 1033.
(18) (a) Matteucci, M. L.; Anyarambhatla, G.; Rosner, G.; Azuma, C.; Fisher, P. E.; Dewhirst, M. W.; Needham, D.; Thrall, D. E. *Clin. Cancer Res.* **2000**, *6*, 3748. (b) Majoros, I. J.; Myc, A.; Thomas, T.; Mehta, C. B.; Baker, J. R. *Biomacromolecules* **2006**, *7*, 572.
(19) Braahler, M.; Georgieva, R.; Buske, N.; Muller, A.; Muller, S.; Pinkernelle, J.; Teichgraber, U.; Voigt, A.; Banmler, H. *Nano Lett.* **2006**, *6*, 2505.
(20) Denis, M. C.; Mahmood, U.; Benoist, C.; Mathis, D.; Weissleder, R. *Proc. Natl. Acad. Sci. U. S. A.* **2004**, *101*, 12634.
(21) Bulte, J. W. *Methods Mol. Med.* **2006**, *124*, 419.
(22) (a) Hu, Y.; Zheng, Z.; Jia, H.; Tang, Y.; Zhang, L. *J. Phys. Chem. C* **2008**, *112*, 13037. (b) Nath, M.; Choudhuri, A.; Kundu, A.; Rao, C. N. R. *Adv. Mater.* **2003**, *15*, 2098.
(23) (a) Oyler, K. D.; Ke, X.; Sines, I. T.; Schiffer, P.; Schaak, R. E. *Chem. Mater.* **2009**, *21*, 3655. (b) Janaki, J.; Kumary, T. G.; Mani, A.; Kalavathi, S.; Reddy, G. V. R.; Rao, G. V. N.; Bharathia, A. *J. Alloys Compd.* **2009**, *486*, 37. (c) Thanikaikarasan, S.; Mahalingam, T.; Raja, M.; Kim, T.; Kim, Y. D. *J. Mater. Sci.: Mater. Electron.* **2009**, *20*, 727.
(24) (a) Feng, Q. J.; Shen, D. Z.; Zhang, J. Y.; Li, B. S.; Lu, Y. M.; Fan, X. W.; Liang, H. W. *App. Phys. Lett.* **2006**, *88*, 012505. (b) Liu, A.; Chen, X.; Zhang, Z.; Jiang, Y.; Shi, C. *Solid State Commun.* **2006**, *138*, 538.
(25) (a) Yu, X.; Yu, J.; Cheng, B.; Huang, B. *Chem.—Eur. J.* **2009**, *15*, 6731. (b) Yu, J.; Dai, G.; Huang, B. *J. Phys. Chem. C* **2009**, *113*, 16394. (c) Yu, J.; Zhang, J.; Liu, S. *J. Phys. Chem. C* **2010**, *114*, 13642.
(26) Tian, G.; Chen, Y.; Zhou, W; Pan, K.; Tian, C.; Huang, X.; Fu, H. *Cryst. Eng. Comm.* **2011**, *13*, 2994.
(27) Yan, M.; Chen, F.; Zhang, J.; Anpo, M. *J. Phys. Chem. B* **2005**, *109*, 8673.
(28) Gericher, H. *Top. Appl. Phys.* **1979**, *31*, 115.
(29) Bessekhouad, Y.; Mohammedi, M.; Trari, M. *Sol. Energy Mater. Sol. Cells* **2002**, *73* (3), 339.
(30) Sun, M.; Li, D.; Li, W.; Chen, Y.; Chen, Z.; He, Y.; Fu, X. *J. Phys. Chem. C* **2008**, *112*, 18076.
(31) (a) Hu, J. S.; Ren, L. L.; Guo, Y. G.; Liang, H. P.; Cao, A. M.; Wan, L. J.; Bai, C. L. *Angew. Chem., Int. Ed.* **2005**, *44*, 1269. (b) Yu, X.; Yu, J.; Cheng, B.; Huang, B. *Chem.—Eur. J.* **2009**, *15*, 6731.
(32) Zhao, J. F.; Song, J. M.; Liu, C. C.; Liu, B. H.; Niu, H. L.; Mao, C. J.; Zhang, S. Y.; Shen, Y. H.; Zhang, Z. P. *CrystEngComm* **2011**, *13*, 5681.
(33) (a) Gao, L.; Zhuang, J.; Nie, L.; Zhang, J. B.; Zhang, Y.; Gu, N.; Wang, T. H; Feng, J.; Yang, D. L.; Perrett, S.; Yan, X. Y. *Nat. Nanotechnol.* **2007**, *2*, 577. (b) Liu, S.; Lu, F.; Xing, R.; Zhu, J. J. *Chem.—Eur. J.* **2011**, *17*, 620. (c) Wei, H.; Wang, E. *Anal. Chem.* **2008**, *80*, 2250.
(34) (a) Tan, X.; Zhang, J.; Tan, S.; Zhao, D.; Huang, Z.; Mi, Y.; Huang, Z. *Electroanalysis* **2009**, *21*, 1514. (b) Zhang, S.; Tang, S.; Lei, J.; Dong, H.; Ju, H. *J. Electroanal. Chem.* **2011**, *656*, 285. (c) Ohnuki, H.; Saiki, T.; Kusakari, A.; Endo, H.; Ichihara, M.; Izumi, M. *Langmuir* **2007**, *23*, 4675.
(35) Dai, Z.; Liu, S.; Bao, J.; Ju, H. *Chem.—Eur. J.* **2009**, *15*, 4321.

(36) Chen, W.; Chen, J.; Liu, A. L.; Wang, L. M.; Li, G. W.; Lin, X. H. *ChemCatChem* **2011**, *3*, 1151.
(37) Kamin, R. A.; Wilson, G. S. *Anal. Chem.* **1980**, *52*, 1198.
(38) Qu, L. H.; Peng, Z. A.; Peng, X. G. *Nano Lett.* **2001**, *1*, 333.
(39) (a) Anuar, K.; Tan, W. T.; Saravanan, N.; Ho, S. M.; Gwee, S. Y. *Pac. J. Sci. Technol.* **2009**, *10*, 801. (b) Thanikaikarasan, S.; Mahalingam, T.; Raja, M.; Kim, T.; Kim, Y. D. *J. Mater. Sci.: Mater. Electron.* **2009**, *20*, 727.
(40) Xin, M.; Li, K. W.; Wang, H. *Appl. Surf. Sci.* **2009**, *256*, 1436.
(41) Dong, Y. Z.; Zheng, Y. F.; Duan, H.; Sun, Y. F.; Chen, Y. H. *Mater. Lett.* **2005**, *59*, 2398.
(42) (a) Bhar, S. K.; Mukherjee, N.; Maji, S. K.; Adhikary, B.; Mondal, A. *Mater. Res. Bull.* **2010**, *45*, 1948. (b) Maji, S. K.; Mukherjee, N.; Dutta, A. K.; Srivastava, D. N.; Paul, P.; Karmakar, B.; Mondal, A.; Adhikary, B. *Mater. Chem. Phys.* **2011**, *130*, 392.
(43) (a) Nair, M. S.; Pena, Y.; Campos, J.; Garcia, V. M.; Nair, P. K. *J. Electrochem. Soc.* **1998**, *114*, 2113. (b) Savadogo, O.; Mondal, K. C. *Sol. Energy Mater. Sol. Cells* **1992**, *26*, 117.
(44) Karaseva, E. I.; Losev, Y. P.; Metelitsa, D. I. *Russ. J. Bioorg. Chem.* **2002**, *28*, 128.
(45) Lineweaver, L.; Burk, D. *J. Am. Chem. Soc.* **1934**, *56*, 658.